L.V. Mokhnatska[1], V.O. Kotsubynsky[1], V.M. Boychuk[1], M.L. Mokhnatskyi[1], Kh.V. Bandura[2], A.I. Kachmar[1], M.A. Hodlevska[1], V.V.Bachuk[3]

Ultrafine β-FeOOH and Fe₃O₄ obtained by precipitation method: comparative study of electrical and electrochemical properties

[1]Vasyl Stefanyk Precarpathian National University, Ivano-Frankivsk, Ukraine, e-mail: liliamokhnatska@gmail.com
[2]Ivano-Frankivsk National Medical University, Ivano-Frankivsk, Ukraine, banduracristina@gmail.com
[3]Ivano-Frankivsk National Technical University of Oil and Gas, Ivano-Frankivsk, Ukraine

In this work, ultrafine powders of β-FeOOH and Fe_3O_4 (specific surface area values are 101 and 135 m^2/g, respectively) have been obtained by precipitation method. Frequency dependences of electrical conductivity was analyzed in the temperature range of 20 - 150 °C. It has been found that the both materials show a superlinear behavior of the frequency dependent electrical conductivity. The values of activation energies for direct current conductivity, cross-over frequency for the electrical conductivity described by Jonscher power law and the superlinear law are 0.55, 0.51 and 0.16 eV for β-FeOOH and 0.22, 0.21 and 0.1 eV for Fe_3O_4, respectively. According to cyclic voltammetry (scan rate in the range of 1-50 mV/s) β-FeOOH material shows a specific capacitance up to 80 F/g, while the one for the Fe_3O_4 material is about 32 F/g. Galvanostatic cycling measurements have been done for discharge currents of 0.05 - 0.25 A/g. The specific energy and power of about 8 W h/kg and 20 W/kg were achieved for the β-FeOOH material when Fe_3O_4 material demonstrate the specific power only up to 3.5 W/kg.

Keywords: iron oxides, super-linear dependence, electrode material, supercapacitor, impedance spectroscopy, electrical conductivity, cyclic voltammetry, specific capacitance.

Received 20 November 2020; Accepted 15 December 2020.

Introduction

Nowadays the improvement of power and energy characteristics of energy storage devices is the important problem, as well as reducing the cost of manufacturing using environmentally friendly materials that can be implemented using large capacities of materials, increasing the cell voltage. Supercapacitors are considered a good solution in the field of electricity storage due to their attractive characteristics, such as long charge-discharge life, low equivalent series resistance (ESR), and high power density [[2]]. Oxides and oxihydroxides of iron are a good solution to meet all the above requirements. Iron oxides have two mechanisms of charge accumulation: EDL capacitance and pseudocapacitance [2].

In this work, ultrafine β-FeOOH and Fe_3O_4 were obtained. The temperature dependence of electrical conductivity is investigated. When approximating the frequency dependences of the real parts of the electrical conductivity by Jonscher power law, an exponent n>1 is obtained, which indicates superlinear behavior. The obtained iron oxides were tested as an electrode material for supercapacitors.

I. Experiment technique

Ultrafine β-FeOOH and Fe_3O_4 powders were obtained by precipitation of iron salts in aqueous solutions. β-FeOOH material was obtained using an aqueous solution of $FeCl_3 \cdot 6H_2O$. The pH = 6.0 - 6.5 was monitored by the addition of 25% ammonium hydroxide (NH_4OH). Fe_3O_4 was obtained using aqueous solutions of $FeCl_3 \cdot 6H_2O$ and $FeCl_2 \cdot 4H_2O$ under the condition of the ratio $Fe^{2+}/Fe^{3+} = 1/2$. Then 25 % ammonium

hydroxide was added to reaction medium and pH = 10.5 - 11.0. Both solutions were kept at 65 °C for 24 h, centrifuged, washed with distilled water and dried at 85 - 95 °C to constant weight. β-FeOOH and Fe₃O₄ were marked as S1 and S2, respectively.

X-ray diffraction analysis. The crystallographic analysis of the samples was performed by XRD powder method using DRON-3.0 diffractometer, equipped with Cu (K_α) radiation. A continuous scan was used to collect 2θ data from 10 to 60 degrees, to determine the crystal structure of the samples. "FullProf" software was used to analyze the XRD patterns.

Porosity of the samples was investigated by nitrogen adsorption method using *NOVA Quantachrome 2200e* adsorption analyzer. Specific surface area values were calculated by BET method.

The impedance measurements on the β-FeOOH and Fe₃O₄ samples were carried out in the temperature range of (20 - 150) °C using Autolab PGSTAT12/FRA-2 spectrometer (frequency of 0.01-100 kHz). The samples were prepared by forming cylinders with a height of 0.3 cm and a cross-sectional area of 2.54 cm² and pressing (the load of 60 kN, used press P-10).

Optical absorption spectra in the wavelength range of 200 - 700 nm were obtained at room temperature using ULAB 102 UV spectrophotometer.

Cyclic voltammetry and galvanostatic measurements were carried on *Autolab PGSTAT/FRA2* workstation using a three-electrode circuit. 1M Li₂SO₄ solution was used as electrolyte. The cell consisted of a working electrode, a reference electrode (Ag/AgCl) and a counter electrode (platinum metal). The working electrode consisted of 85 wt.% active material, 10 wt.% acetylene carbon black and 5 wt.% polyvinylidene fluoride in N-methylpyrrolidone applied to a nickel mesh. Electrochemical studies were performed in the potential range from -0.85 to -0.1 V.

II. Results and Discussion

β-FeOOH and Fe₃O₄ powders with tunnel and spinel structure, respectively, were obtained by precipitation method. A similar synthesis method is described in [3] According to XRD analysis, the material S1 has a structural ordering for β-FeOOH (JCPDS #34-1266) [4]. Compared to the (400) and (211) reflexes, (310) reflex broadening is observed. This fact may indicate rod-shaped particles with an akaganeite structure [5]. For S2, material the XRD pattern indicates a state close to amorphous with a hint of spinel structure as it is evidenced by the maximum intensity of (311) reflex [6] (Fig. 1).

Fig. 2. shows the frequency dependences of the specific electrical conductivity and the frequency dependences of the real electrical conductivity component (in the temperature range of 20 - 150 °C) for the β-FeOOH and Fe₃O₄ samples. For S1 material, the electrical conductivity increases monotonously (to a frequency values of 10² - 10³ Hz) with increasing current frequency for real part of electrical conductivity and total electrical conductivity. At the same time the frequency dependences of the total electrical conductivity for the
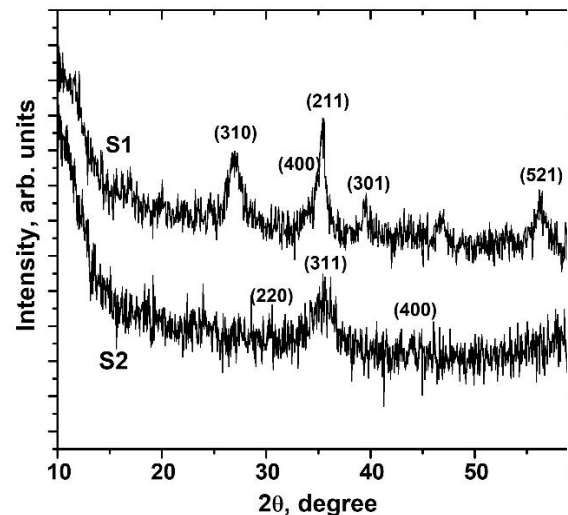

Fig. 1. XRD patterns of materials of S1 and S2 systems.

sample S2 are characterized by a peak at certain frequencies for each temperature value (Fig. 2b.).

Both samples have a nonlinear temperature dependence of the electrical conductivity. For sample S1, the electrical conductivity increases up to temperature of 100 °C and then decreases at the temperature of 150 °C (Fig. 2, a, c). Sample S2 shows the presence of a maximum at the temperature of 75 °C with a subsequent decrease in electrical conductivity (Fig. 2, b, d).

For ferrites, the change in temperature affects the mobility of charge carriers and has almost no effect on the concentration of such carriers. Charge carriers are localized on magnetic ions (iron ions). Thus, electrical conductivity is provided by the exchange of 3d electrons between Fe^{2+} and Fe^{3+}. The hopping mechanism of electrical conductivity is predominant. [7].

The frequency dependences of the real part of the conductivity for the β-FeOOH and Fe₃O₄ were interpreted using the Jonscher's power law (JPL) [8]: $\sigma(\omega) = \sigma_{dc} + A\omega^n$, where σ_{dc} is a frequency independent component of electrical conductivity, A and *n* are constants. The exponent n is a measure of the strength of the ionic interaction and characterizes the deviation from the Debye behavior [8]. From JPL fittings the exponent n of fractal-power law is obtained. A value of $1 < n < 2$ (Fig. 3) indicates that the sample shows a superlinear behavior and can be described by superlinear power law (SPL).

The change of n with temperature characterizes the change in the degree of interaction of moving ions and the lattice around them (Fig. 3). The decrease in *n* with temperature increasing (at 20-50°C for S1 sample and at 20 - 100 °C for S2 sample) is the evidence that percolation mechanism of large polarons is predominant [10]. The change in parameter *n* can be caused by localization and delocalization effects of charge carriers.

It is possible under the condition if electrons energy is less than electrostatic energy, applied to borders between grains. The formation of Fe^{3+}-O-Fe^{2+} chains provides the formation of electrical conductivity

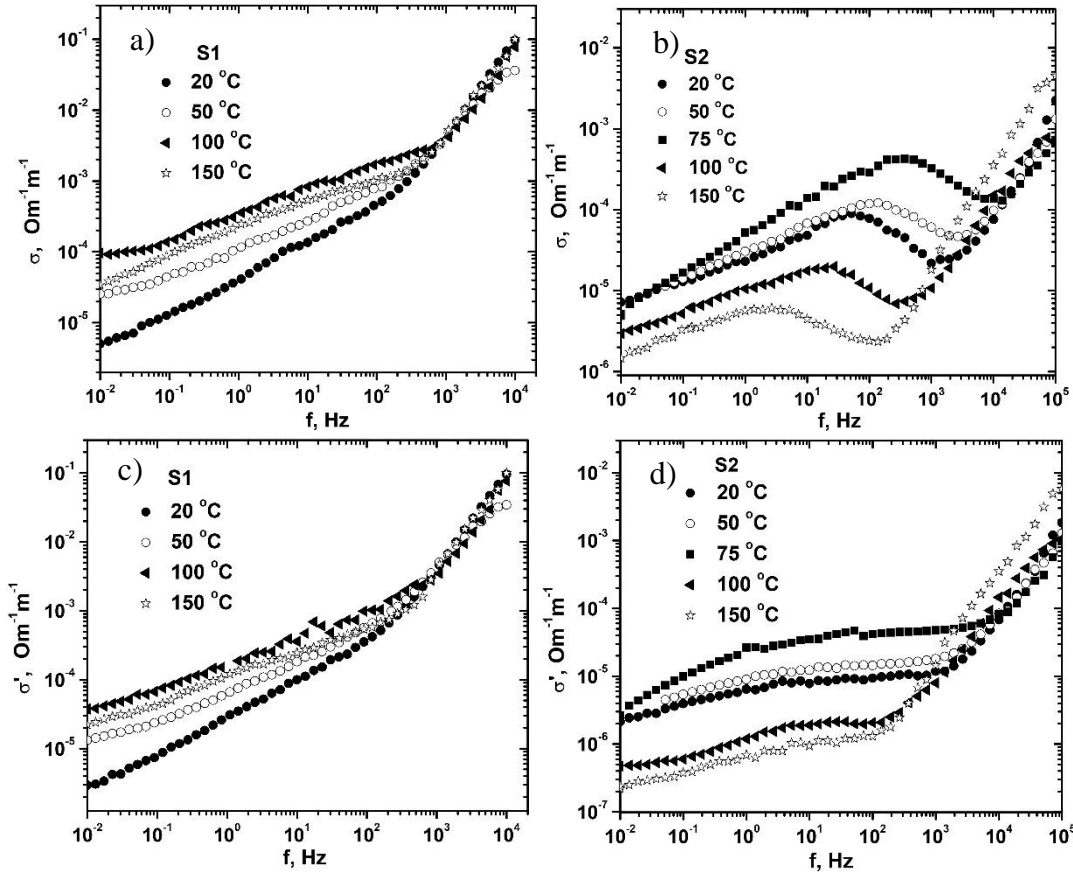**Fig. 2.** The ac conductivity (σ) dependencies (a, b) and the real part of electrical conductivity (σ') spectra (c, d) for S1 and S2 at different temperatures.
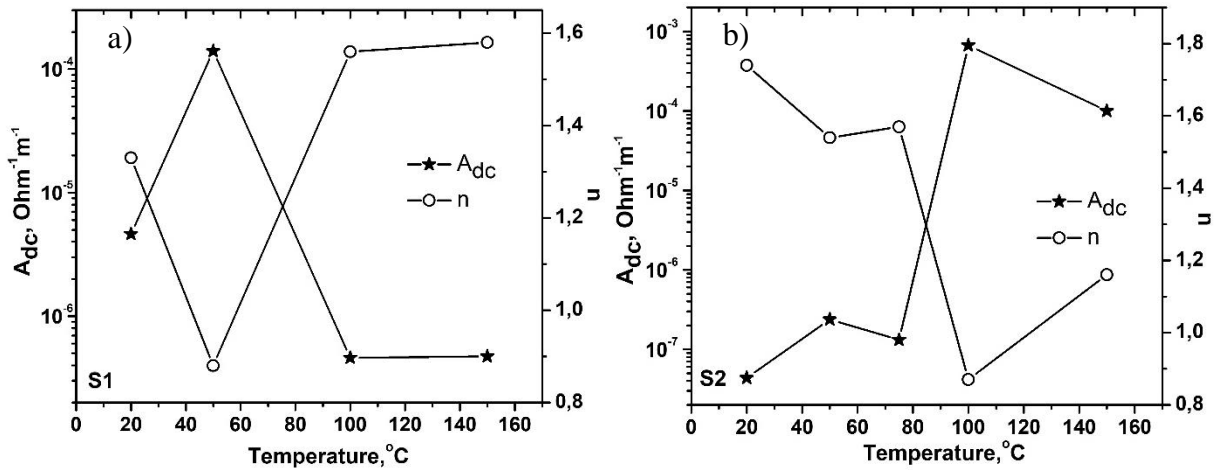

Fig. 3. Dependence of characteristic parameters (A and n) on the power law of Jonscher on the temperature for β-FeOOH (a) and Fe_3O_4 (b).

channels for localized d-electrons transitions.

SPL behavior is the best demonstrated by the dependences of dielectric losses on frequency $\varepsilon''(f)$, $\varepsilon''(\nu) = \dfrac{\sigma'}{2\pi\varepsilon_0\nu}$, where ε_0 is the dielectric constant, $\varepsilon''(\omega)$ is an imaginary part of complex dielectric constant. The presence of minimum in the frequency response separates the JPL and SPL behaviors [[11], [12]] (Fig. 4).

When $1 < n < 2$ the conductivity spectra can be described by a modified JPL as:

$$\sigma'(\omega) = \sigma_{dc} + A(T)\omega^n + B(T)\omega^m \qquad (1)$$

where σ_{dc} is dc conductivity, the second term with $n < 1$ indicates the JPL behavior and third term B(T) is temperature dependent parameter with $m > 1$ indicates SPL behavior, due to two level systems [[13]] or low-energy excitation modes of vibrations [[14]].

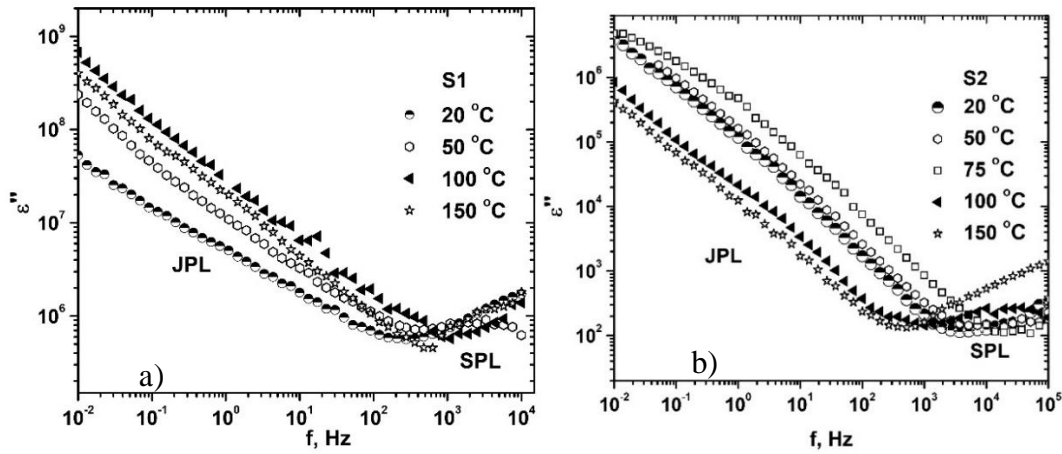Modified law, to describe the real part of ac conductivity [15]:

Fig. 4. Frequency dependence of dielectric loss for β-FeOOH (a) and Fe$_3$O$_4$ (b) at different temperatures; the presence of minimum in the frequency response separates the JPL and SPL behaviors.

$$\sigma'(\omega) = \sigma_{dc}\left[1 + (\omega/\omega_{p1})^n + (\omega/\omega_{p2})^m\right] \qquad (2)$$

where, ω_{P1} is cross-over frequency from dc to JPL and ω_{P2} is cross-over frequency from JPL to SPL. The temperature dependences of σ_{dc}, ω_{P1} and ω_{P2} show Arrhenius behavior as follow:

$$\sigma_{dc}T = \sigma_0 \exp(-E_{dc}/k_BT) \qquad (3)$$

$$\omega_{p1} = \omega_{01}\exp(-E_{p1}/k_BT) \qquad (4)$$

$$\omega_{p2} = \omega_{02}\exp(-E_{p2}/k_BT) \qquad (5)$$

where T is an absolute temperature, E_{dc}, E_{P1} and E_{P2} are activation energy at constant electrical conductivity, cross-over frequency for JPL and cross-over frequency for SPL, respectively, k_B is Boltzmann's constant.

According to Coupe's theory [16],[17], the electrical conductivity of ferrites shows a dispersion at frequencies above 10^4 Hz, which indicates the presence of grains with high electrical conductivity, and intergranular boundaries with a high resistance value. The hopping energy can be calculated as: $W_H = E_\mu + E_\sigma$, where $E\mu$ is a thermal energy of motion activation E_σ is an activation energy of electrical conductivity according to the band theory of semiconductors, which is calculated by the Arrhenius equation: $\sigma_{dc}(T) = \sigma_0 \exp\left[-\dfrac{E_\sigma}{kT}\right]$. The hopping energy W_n coincides with the energy E_{dc} of the transition from dc to JPL. The frequency ω_{p1} was determined from $\ln\sigma$ vs $\ln f$ plot (Fig. 5). Where ω_{p1} is the point of intersection of two linear areas (shown by dashed lines) as in [18].

The cross-over frequency ω_{p1} for the material Fe$_3$O$_4$, coincides with the peak frequency of total electrical conductivity in Fig.2 b. The cross-over frequency ω_{p2} was determined from frequency dependence of dielectric loss (the minimum in the plot) (Fig. 4.).

All Arrhenius plots were linearized in the temperature range of 20-100°C for material β-FeOOH and 20-75°C for material Fe$_3$O$_4$ (Fig. 6, a, c) and (Fig. 6, b, d). The calculated energies Wn, Eσ, Edc, E$_{P1}$, E$_{P2}$ are given in Table 2.

The authors [19] obtained similar relationships between the values of activation energies E_{dc}, E_{P1} and E_{P2}.
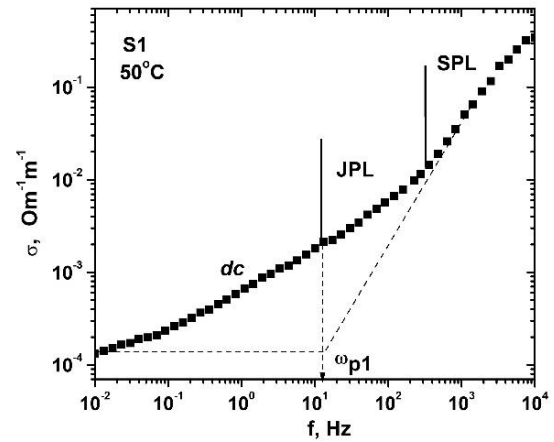

Fig. 5. Frequency dependence of electrical conductivity for sample S1 at 50 °C (the same data as in Fig. 1), which demonstrates the frequency of transition from constant electrical conductivity to the JPL area and to the SPL area.

Table 1

The cross-over frequency ω_{p1} and ω_{p2} for samples β-FeOOH and Fe$_3$O$_4$

Temperature, °C	ω_{p1}, Hz β-FeOOH	ω_{p1}, Hz Fe$_3$O$_4$	ω_{p2}, Hz β-FeOOH	ω_{p2}, Hz Fe$_3$O$_4$
20	3,4	72	272	3727
50	12,3	139	480	5180
75		268		7197
100	255	27	1096	1000
150	55	2,4	630	372

Table 2

Activation energies obtained from Arrhenius plots for β-FeOOH and Fe$_3$O$_4$ materials

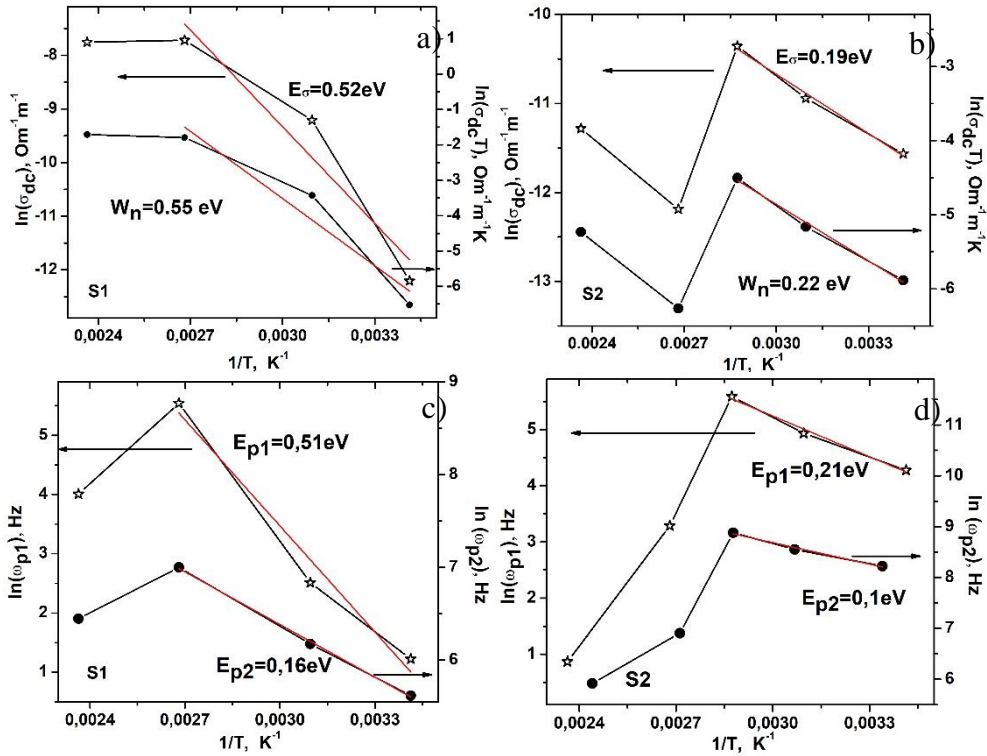| Sample	W_n, E_{dc}	E_σ	E_{P1}	E_{P2}
β-FeOOH	0.55 eB	0.52 eB	0.51 eB	0.16 eB
Fe$_3$O$_4$	0.22 eB	0.19 eB	0.21 eB	0.1 eB

Fig. 6. Arrhenius behavior of hopping mechanism of charge transfer and of cross-over frequency from dc to JPL and from JPL to SPL for β-FeOOH and Fe_3O_4 samples.
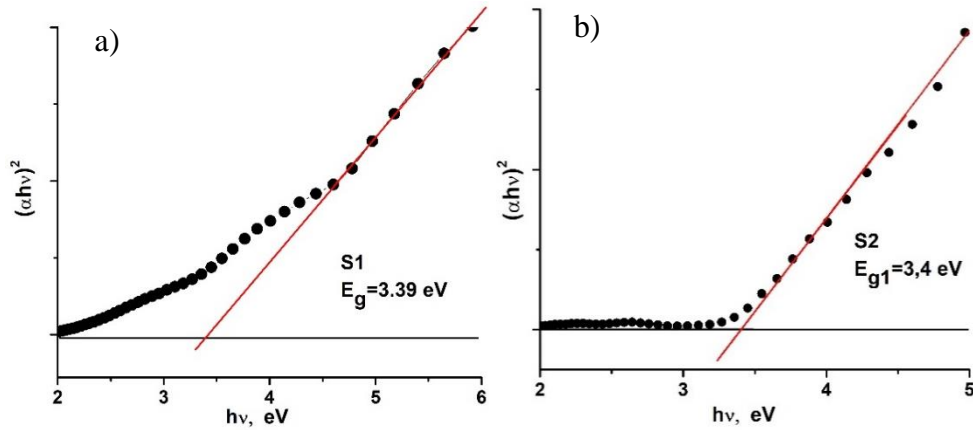

Fig. 7. – Determination of the optical band gap energy for direct transition E_{g1}^{opt} for S1 and S2.

The behavior of SPL is theoretically described by the double asymmetric potential well (ADWP) model. Standard ADWP is used in the field of low frequencies and low temperatures [20]. However, the authors of [21] noted that it is applicable at high temperatures. It is based on the assumption that in the system a group of atoms/ions occupies one of the two non-equivalent energy positions. The activation energies E_{P1} and E_{P2} are the energy of the height of the energy barriers of the asymmetric well, and their difference is the energy of asymmetry.

The band gap width energy E_g for S1 and S2 samples was calculated from the Tauc model. The exponential dependence of the adsorption coefficient α corresponds to the empirical equation:

$$\alpha = \frac{const}{h\nu}[h\nu - Eg]^m \qquad (6)$$

where h is Planck's constant, ν is frequency of incident light, m = 1/2 i 2 for direct and for indirect transition, respectively. By plotting $(\alpha h\nu)^2$ as a function of photon energy ($h\nu$), the optical energy band gap for direct E_{g1}^{opt} transition was determined. For S1 sample, the band gap is 3.39 eV, which is more than the band gap for bulk akaganeite (Eg about 2.0-2.1 eV [22], [23]). For this sample there is a direct-band optical transition.

The CVA curves (Fig. 8) of the obtained β-FeOOH electrode have a rectangular shape at low scan rate values. This indicates the contribution of the PES mechanism of charge accumulation. As the scan rate
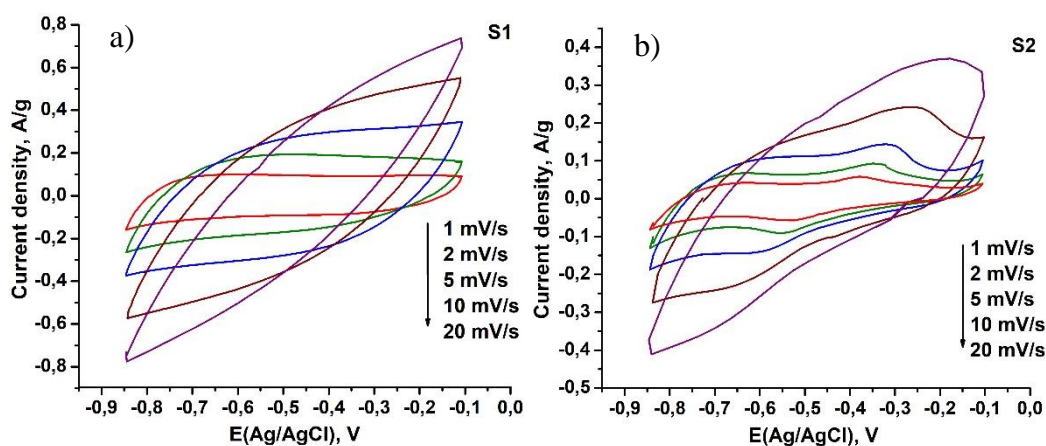
Fig. 8. CVA of the β-FeOOH/Li$_2$SO$_4$ and Fe$_3$O$_4$/Li$_2$SO$_4$ systems for scan rates from 1 to 20 mV/s.

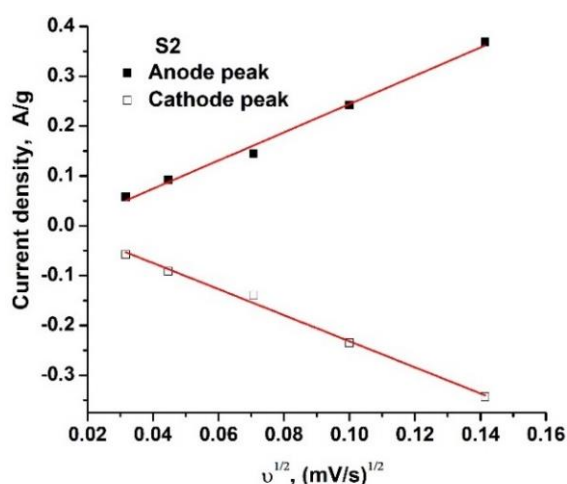**Fig. 9.** $i_p(\upsilon^{1/2})$ dependence for the electrode material Fe$_3$O$_4$.

increases, the CVA curve transforms into an elliptical one, which is caused by the contribution of the pseudocapacitive component. The CVA curves of the obtained Fe$_3$O$_4$ electrode show two slight redox peaks (anode and cathode), which indicates the process of Faraday reactions on the electrode surface. Redox processes in electrolytes are caused by transitions Fe^{3+}↔Fe^{2+}:

$$Fe_3O_4 + 8H^+ + 2e^- \leftrightarrow 3Fe^{2+} + 4H_2O$$
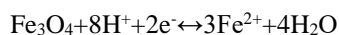
There is a visible growth in peak current densities with increasing of scan rates, this indicates a sufficient rate of transport during the redox reaction. While, the anode peak moves towards higher potentials, and the cathode peak shifts to lower potential values. The reason is that with increase in scan rate, the irreversibility of the process increases.

Fig. 9 shows a linear dependence of i_p ($\upsilon^{1/2}$), which indicates the "depletion" of the electrode capacitance and redox surface processes are diffusion-limited. This is characteristic of quasi-reversible electrochemical reactions described by the Randles-Shevchik equation [24]: $i_p = 2.69 \times 10^5 n^{3/2} A \Delta C D^{1/2} \upsilon^{1/2}$ (at 25 °C), where i is

the peak current, A is an area of working electrode (cm^2), n is a number of electrons, ($n = 1$ for the case of a reaction Fe^{3+} ↔ Fe^{2+}), D is an ion diffusion coefficient Li$^+$ (cm^2/s), υ is a scan rate (V/s), C is an ion concentration Li$^+$ in the electrolyte. The calculated diffusion coefficients of Li$^+$ ions for the subsurface layer Fe$_3$O$_4$ are given in Table 3.

The Figure 10 shows the dependence of the specific capacitance on the scan rate calculated from CVA for β-FeOOH and Fe$_3$O$_4$ materials. The value of the specific capacitance decreases monotonically. The maximum of

Table 3

Diffusion coefficients at different scan rates

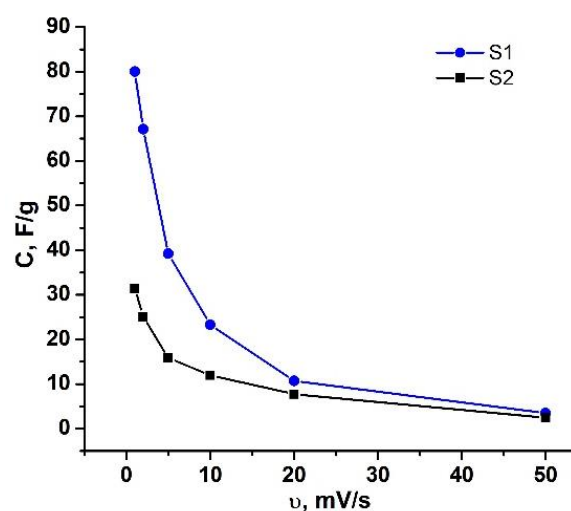| Scan rate, mV/s	Diffusion coefficient at discharge process, cm$^2 \cdot$s^{-1}	Diffusion coefficient at charge process, cm$^2 \cdot$s^{-1}
1	5,55·10^{-13}	4,91·10^{-13}
2	8,69·10^{-13}	7,68·10^{-13}
5	2,19·10^{-12}	1,94·10^{-12}
10	3,82·10^{-12}	3,39·10^{-12}
20	9,2·10^{-12}	8.13·10^{-12}

Fig 10. Specific capacitance of the β-FeOOH /Li$_2$SO$_4$ system at scan rates from 1 to 50 mV/s.
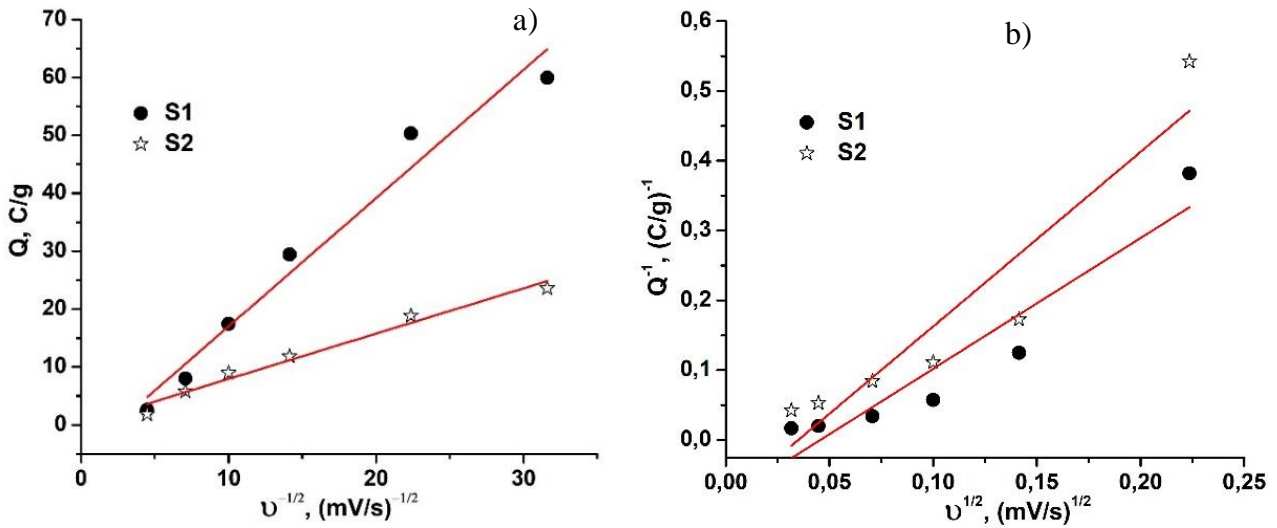
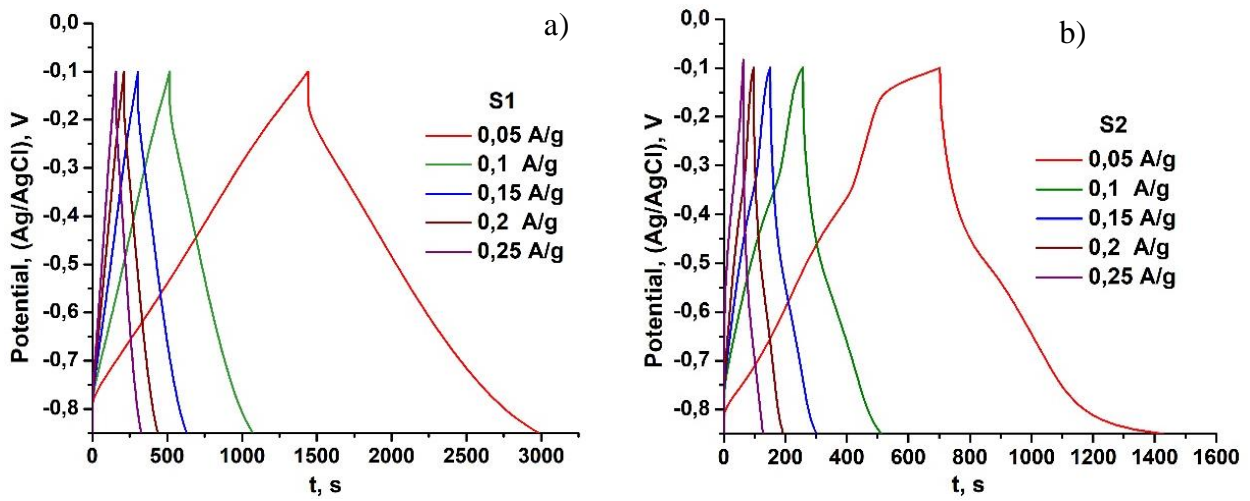**Fig. 11.** Dependence of functions $Q(v^{-1/2})$ (a) and $Q^{-1}(v^{1/2})$ (b).

Fig. 12. Charge/discharge curves for β-FeOOH and Fe_3O_4 at different values of current densities

the specific capacitance is 80 F/g for β-FeOOH and 32 F/g for Fe_3O_4 at scan rate of 1 mV/s.

The redistribution of the contribution to the total capacitance of the materials of the EDL capacitance and the Faraday capacitance was calculated using the ratio: $Q = Q_{v=\infty} + \alpha v^{-\frac{1}{2}}$, $Q^{-1} = Q_{v=0}^{-1} + b v^{\frac{1}{2}}$, where Q is total charge calculated at different values of scan rate ($Q = Cm\Delta U = \dfrac{s}{2v}$, S is the total area of the voltaic curves), $Q_{v=0}$ is a maximum total charge, $Q_{v=\infty}$ is a double layer charge, a and b are constants. The experimental dependences $Q(v^{-1/2})$ and $Q^{-1}(v^{1/2})$ are approximated by linear functions (Fig. 11). The contribution of EDL capacitance to the total capacity is 44 % and 14 % for S1 and S2, respectively.

Galvanostatic measurements (Fig. 12) were performed at the applied specific currents of 0.05 A/g - 0.25 A/g, in increments of 0.05 A/g. A slight plateau is observed in the discharge curve for sample S2 at a current charge/discharge of 0.05 A/g in the potential range of -0.5 - -0.6V. This behavior of the discharge curve is a result contribution of pseudocapacitance and

meets the recovery process.

The Figure 13 shows the dependence of the specific capacitance on the discharge current density calculated from charge/discharge curves of materials β-FeOOH and Fe_3O_4. The capacitance of the charge/discharge curves is calculated by the formula: $C_{spec} = I\Delta t\, mU$, where I is the direct discharge current, m is the mass of active materials (g), Δt is the discharge time, ΔU is the potential discharge window. The capacitance of β-FeOOH is higher than the capacitance of Fe_3O_4, which correlates with the CVA data. The maximum of the specific capacitance is 104 F/g for β-FeOOH and 46 F/g for Fe_3O_4 at a discharge current density of 0.05 A/g.

Specific energy and specific power are important for the practical use of materials. The values of specific energy and average specific power are calculated by: $E_{spec} = C_{spec}U^2 / 2$ and $W_{spec} = E_{spec} / t$, where C is the capacitance calculated from the galvanostatic study, U is the range of potentials in which the survey was performed, t is the discharge time. Material S1 has higher values of specific energy than material S2. The maximum specific energy for material S2 is about 8 W h/kg at a value of specific power equal to 20 W/kg.
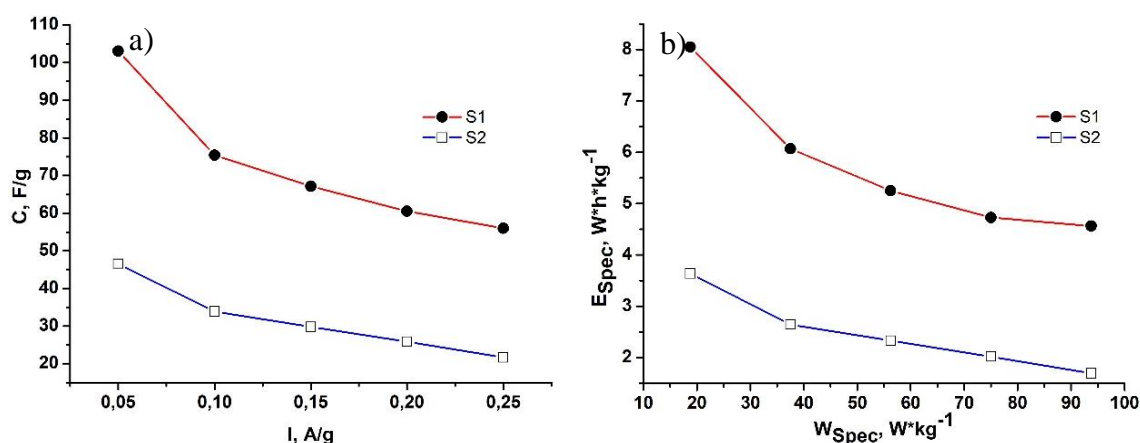
Fig. 13. Dependence of specific capacitance for S1 and S2 materials on current density (a) and Ragone plot (b) for S1 and S2 electrode**s**.

Conclusions

Ultrafine powders of β-FeOOH and Fe₃O₄ were obtained by precipitation method, that is identified by X-rays analysis. Temperature dependences of electrical conductivity for materials β-FeOOH and Fe₃O₄ were investigated. It was established that the frequency dependences of the electrical conductivity showed superlinear behavior. It was established that the value activation energies for dc conduction, cross-over frequency for JPL and cross-over frequency for SPL were: $E_{dc} = 0.55$ eV, $E_{p1} = 0.51$ eV, $E_{p2} = 0.16$ eV and $E_{dc} = 0.22$ eV, $E_{p1} = 0.21$ eV, $E_{p2} = 0.1$ eV for β-FeOOH and Fe₃O₄, respectively. Moreover, β-FeOOH and Fe₃O₄ materials were used as electrode materials. Specific capacitance for β-FeOOH is equal to 80 F/g at a scan rate value of 1 mV/s, while the specific capacitance for Fe₃O₄ is 32 F/g.

Mokhnatska L.V. – PhD student, of the Department of Material Science and New Technology;
Kotsubynsky V.O. – Professor, Doctor of Physical and Mathematical Sciences;
Boychuk V.M. – Professor, Doctor of Physical and Mathematical Sciences;
Mokhnatskyi M.L. – PhD student, of the Department of Material Science and New Technology;
Bandura Kh.V. – PhD, assistant of the Department of Medical Informatics, Medical and Biological Physics;
Kachmar A. I. – PhD of the Department of Material Science and New Technology;
Hodlevska M.A. – Ph.D student of the Department of Material Science and New Technology;
Bachuk V.V. – PhD, assistant of the Department.

[1]   B.E. Conway, Electrochemical Super capacitor and Technological Applications. (Kluwer-Plenum Press, New York, 1999).
[2]   A.J. Burke, Power Sources 91, 37 (2000) (doi.org/10.1016/S0378-7753(00)00485-7).
[3]   L.V. Mokhnatska, V.O. Kotsyubynsky, A. Hrubyak, S.V. Fedorchenko, S.I. Vorobiov, Journal of Nano-and Electronic Physics 10(3), 03029 (2018) (10.21272/jnep.10(3).03029).
[4]   X. Rao, X. Su, C. Yang, J. Wang, X. Zhen, D. Ling, Cryst. Eng. Comm. 15(36), 7250 (2013) (doi.org/10.1039/C3CE40430G).
[5]   D.N. Bakoyannakis, E.A. Deliyanni, A.I. Zouboulis, K.A. Matis, L. Nalbandian, T. Kehagias, Microporous and Mesoporous Materials 59(1), 35 (2003) (doi.org/10.1016/S1387-1811(03)00274-9).
[6]   Y.X. Chen, L.H. He, P.J. Shang, Q.L. Tang, Z.Q. Liu, H. Liu, L.P Zhou, Journal of Materials Science and Technology 27(1), 41 (2011).
[7]   H. Hosseinpour, A. Sadeghi, Morisako, Journal of Magnetism and Magnetic Materials 316(2), e283 (2007) (doi.org/10.1016/j.jmmm.2007.02.119).
[8]   I.I. Popov, R.R. Nigmatullin, A.A. Khamzin, I.V. Lounev, Journal of Physics: Conference Series 394, 12 (2012) (doi: 10.1063/1.4764343).
[9]   J.R. Macdonald, Solid State Ionics 133(1-2), 79 (2000) (doi.org/10.1016/S0167-2738(00)00737-2).
[10]   J.C. Dyre, T.B. Schroder, Rev. Mod. Phys. 72(3), 873 (2000) (doi.org/10.1103/RevModPhys.72.873).
[11]   . S.K. Mandal, S. Singh, P. Dey, J.N. Roy, P.R Mandal, T.K. Nath, Philosophical Magazine 97(19), 1628 (2017) (doi.org/10.1080/14786435.2017.1312021),
[12]   D.P. Singh, K. Shahi, K. Kar. Kamal, Solid State Ionics 287, 89 (2016) (doi.org/10.1016/j.ssi.2016.01.048).
[13]   A.K. Jonscher, Nature 267, 673 (1977).

[14] J. Dieckhöfer, O. Kanert, R. Küchler, A. Volmari, Phys. Rev. B 55, 14836 (1997) (doi.org/10.1103/PhysRevB.55.14836).

[15] P. Almond, G. K. Duncan, A. R. West, Solid State Ionics, 8, 159-164 (1983) (doi.org/10.1016/0167-2738(83)90079-6).

[16] A. Radoń, D. Łukowiec, M. Kremzer, J. Mikuła, P. Włodarczyk, Materials 11(5), 735 (2018) (doi.org/10.3390/ma11050735).

[17] M. Sertkol, Y. Kōseoglu, A. Baykal, J. Magn, Journal of Magnetism and Magnetic Materials 322(7), 866 (2010) (doi.org/10.1016/j.jmmm.2009.11.018).

[18] J.P. Tiwari, K. Shahi, Philosophical Magazine 87(29), 4475 (2007) (doi.org/10.1080/14786430701551913).

[19] R. Cheruku, G. Govindaraj, V. Lakshmi, Materials Chemistry and Physics 146(3), 389 (2014) (doi: 10.1016/j.matchemphys.2014.03.043).

[20] S. Nowick, B. SLim, A.V. Vaysleyb, A.S. Nowick Solids 172-174(2), 1243 (1994).

[21] D.P. Singh, K. Shahi, K. Kar. Kamal, Solid State Ionics 287, 89 (2016) (doi.org/10.1016/j.ssi.2016.01.048).

[22] R.M. Cornell, U. Schwertmann, The Iron Oxides: Structure, Properties, Reactions, Occurrences, and Uses, (John Wiley & Sons, Weinheim, Germany, 2nd edition, 2003).

[23] J.K. Leland, A.J. Bard, Journal of Physical Chemistry 91(19), 5076 (1987) (doi.org/10.1021/j100303a039).

[24] B.B. Li, Y.Q. Liang , X.J. Yang , Z.D. Cui, S.Z. Qiao, S.L. Zhu, K. Yin, Nanoscale 7(40), 16704 (2015) (doi.org/10.1039/C5NR04666A).

Л.В. Мохнацька[1], В.О. Коцюбинський[1], В.М. Бойчук[1], М.Л. Мохнацький[1], Х.В. Бандура[2], А.І. Качмар[1], М.А. Годлевська[1], В.В. Бачук[3]

Ультрадисперсні β-FeOOH та Fe$_3$O$_4$, отримані методом осадження: порівняльний аналіз електричних та електрохімічних властивостей

[1]*Прикарпатський національний університет імені Василя Стефаника, Івано-Франківськ, Україна, e-mail: liliamokhnatska@gmail.com*
[2]*Івано-Франківський національний медичний університет, Івано-Франківськ, Україна, banduracristina@gmail.com*
[3]*Івано-Франківський національний технічний університет нафти і газу, Івано-Франківськ, Україна*

Ультрадисперсні порошки β-FeOOH та Fe$_3$O$_4$ з питомими площами поверхні 101 та 135 м^2/г, відповідно, отримувалися методом осадження. Частотні залежності (10^{-2} - 10^5 Гц) питомої провідності цих матеріалів аналізувалися в діапазоні температур 20 - 150 ℃. Встановлено, що обидва матеріали проявляють суперлінійну поведінку частотної залежності питомої провідності. Енергії активації провідності для постійного струму, переходу до електричної провідності, що описується степеневим законом Джоншера та переходу до суперлінійної поведінки провідності, складають 0,55; 0,51 і 0,16 еВ та 0,22; 0,21 і 0,1 еВ для зразків β-FeOOH та Fe$_3$O$_4$, відповідно. За даними циклічної потенціометрії при зміні швидкості сканування в діапазоні від 1 - 50 мВ/с матеріал β-FeOOH демонструє питому ємність до 80 Ф/г, в той час як ємність матеріалу Fe$_3$O$_4$ сягає 32 Ф/г. Гальваностатичні вимірювання проводились для струмів розряду 0,05 - 0,25 А/г. Для матеріалу β-FeOOH досягається максимальна питома енергія 8 Вт год/кг при значенні питомої потужності 20 Вт/кг, для матеріалу Fe$_3$O$_4$ до 3,5 Вт/кг.

Ключові слова: оксиди заліза, суперлінійна залежність, електродний матеріал, суперконденсатор, імпедансна спектроскопія, електропровідність, циклічна вольтамперометрія, питома ємність.